The topology of the adiabatic passage process for molecular photodissociative dynamics

2008 J. Phys. A: Math. Theor. 41 145303

(http://iopscience.iop.org/1751-8121/41/14/145303)

IOP PUBLISHING JOURNAL OF PHYSICS A: MATHEMATICAL AND THEORETICAL

J. Phys. A: Math. Theor. **41** (2008) 145303 (25pp) doi:10.1088/1751-8113/41/14/145303

The topology of the adiabatic passage process for molecular photodissociative dynamics

David Viennot[1], **Georges Jolicard**[1] **and John P Killingbeck**[1,2]

[1] Observatoire de Besançon-Institut UTINAM (CNRS UMR 6213, Université de Franche-Comté), 41 bis Avenue de l'Observatoire, BP1615, 25010 Besançon cedex, France
[2] Centre for Mathematics, University of Hull, Hull HU6 7RX, UK

E-mail: viennot@obs-besancon.fr and george@obs-besancon.fr

Received 21 August 2007, in final form 29 February 2008
Published 26 March 2008
Online at stacks.iop.org/JPhysA/41/145303

Abstract

We study population transfer processes for photodissociation, as described within the optical potential model, in the context of adiabatic or quasi-adiabatic dynamics. By a reformulation of the adiabatic passage theory in terms of the fibre bundle topology, we extend the analysis made by Yatsenko *et al* (2002 *Phys. Rev.* A **65** 043407) from conservative to dissipative systems. We show that this topology is associated with the problem of eigenvalue labelling and hence with the continuous eigenvalue following process in the control parameter space. Problems involving adiabatic passage, the direct chirping process and non-adiabatic transitions are studied, with particular regard to the presence of resonance states. We also discuss the role played by the molecular continua.

PACS numbers: 33.80.Be, 33.80.Gj, 03.65.Vf

1. Introduction

In 2002, Yatsenko *et al* [1] proposed a method for the analysis of quantum dynamical systems in the strong adiabatic regime. Their 'topology of adiabatic passage' method is well adapted to study complete population transfer between bound states of an atom or molecule in strong electromagnetic fields. It extends a previous theory which describes atoms interacting with laser fields, the adiabatic Floquet theory [2]. The method proposed by Yatsenko *et al* is based on the visualization of the path $\mathcal{C}$ describing the field evolution, as drawn on the eigenvalue surfaces. By considering the topology of these surfaces and their contacts point (the crossings), it is possible to understand the behaviour of the dynamical system in a strong adiabatic regime, i.e. a regime without non-adiabatic transitions. In these strong adiabatic regimes, the state of the dynamical system remains projected on the same eigenvector until the path $\mathcal{C}$ passes close to an eigenvalue crossing point $\vec{R}_0$. At this moment, the dynamical system suddenly makes a transition between energy surfaces. This analysis is applied in [1] to some dynamical processes

involving two- and three-level atoms. In the electromagnetic picture of adiabatic dynamics, the sudden transition is simply due to the meeting of the path $\mathcal{C}$ with a magnetic monopole (see [3] for a brief presentation of the magnetic monopole theory). The analogy between magnetic monopole theory and the mathematical structure describing the energy crossing in the adiabatic framework is now currently used throughout the atomic and molecular physics literature, see [4–11].

In this paper we explore the topology of population transfer processes which involve resonance states. The method described in [1] is restricted to a conservative system (with only bound states) controlled by two parameters, because it needs the analysis of a three-dimensional graph (real eigenvalues varying with respect to two parameters). But for resonances, this method needs the analysis of a four-dimensional graph (complex eigenvalues varying with respect to two parameters). We show in this paper that the adiabatic passage topology is in fact the topology of the adiabatic bundle describing the Berry phase. We propose a method to visualize this topology by means of a graph with a dimension equal to the number of control parameters. We can then apply the method to dissipative systems (resonances) controlled by two parameters and to conservative and dissipative systems controlled by three parameters. We show that the topology of the adiabatic bundle (and thus the topology of the adiabatic passage) is related to the problem of the eigenvalue labelling with respect to the control parameters, a point which has not previously been made in the literature on Berry phases. We show that the topology is much more complicated in the dissipative case. We should note that we do not need to restrict our attention to strong adiabatic regimes, because the adiabatic bundle topology can also describe non-adiabatic transitions occurring in weak adiabatic regimes.

Another important point concerns the meaning which is given in our study to the term 'adiabatic regime'. After the pioneering work of Berry [12], who illustrated the geometric phase concept for a spin in a magnetic field, many works have been concerned with the electronic wavefunctions which depend adiabatically on the classical evolution of the nuclear coordinates in the Born Oppenheimer approximation [13, 14]. In these publications the topological effect is associated with a spatial system of coordinates, i.e. to the configuration space, and the classical manifold which defines the static geometry is related to the classical nuclear motions which are very slow compared with the electronic motions. In this framework, the relations between time-dependent magnitudes in the adiabatic limit and time-independent magnitudes have been analysed in [15], which treats molecular Born Oppenheimer systems.

Our paper is devoted to a different problem. Our goal is to show the topological effects due to the modulations of the amplitude and the frequency of a laser field interacting with a molecule (somewhat as done by the works of Yatsenko *et al* [1] in the context of atomic physics). This point of view is consistent with that of the experimentalists performing laser-control experiments. The vibrational wavefunction depends on the laser parameters, which constitute a classical manifold. Thus the laser modulations vary very slowly compared to the movements of the nuclei, which are considered as quantum particles. The problem concerning the electronic states as a function of internuclear distance is thus considered as already having been solved seperately in the Born Oppenheimer approximation. The solution of this preliminary problem gives our starting data, the vibrational potential surfaces associated with the electronic states and the electronic transition dipole moments.

Many works have analysed reactive atom–diatom collision processes [16] and the dissociation, ionization and Coulomb explosion of diatomic molecules in strong laser fields [17–19]. Here we do not consider very strong laser field amplitudes. Our approach is illustrated by studying inelastic radiative transitions and the photodissociation of diatomic molecules, as produced by laser pulses of intensity $I < 10^{13}\,\mathrm{W\,cm^{-2}}$, for which it is assumed that ionization is not present. A large part of our interest is thus focused on the adiabatic behaviour of these

open systems and on the precise role played by resonance states and molecular continua in photodissociation processes.

This paper is organized as follows. Section 2 reviews some basic concepts concerning the modelling of molecular processes, adiabaticity and the Berry phase phenomenon. Section 3 extends some results concerning bound states to the case of resonance states. Finally, section 4 discusses the role of the continuum in adiabatic processes. In order to help the reader to compare the conservative case with the dissociative case, and thus to better appreciate the emphasis of the present paper, an appendix sets out the analysis of the topology of the adiabatic passages between bound states in terms of the fibre bundle topology.

2. Modelling molecular processes and adiabaticity

2.1. The photodissocative Hamiltonian

This section presents some general aspects of the modelling of molecular processes and of the concept of adiabaticity. It recalls some results which are needed for the understanding of later sections and also fixes the notation. In order to simplify the analysis we consider a one-dimensional molecular vibrational problem (i.e. a diatomic molecule or a single bond), the generalization to multidimensional vibrations being straightforward. We thus consider the self-adjoint Hamiltonian of the isolated molecule

$$H_0 = -\frac{\hbar^2}{2m}\frac{\mathrm{d}^2}{\mathrm{d}r^2} + V(r) \tag{1}$$

acting on the r-dependent wavefunctions, where r is the internuclear distance, m is the molecular reduced mass and V is the vibrational potential (or possibly several potentials, depending on the electronic state).

In the general case, the spectrum of H_0 is composed of a pure point part and a continuous part: $\mathrm{Sp}(H_0) = \mathrm{Sp}_{pp}(H_0) \cup \mathrm{Sp}_{\mathrm{cont}}(H_0)$. The photodissociation process can be then viewed as a transfer from a state associated with $\mathrm{Sp}_{pp}(H_0)$ to a state associated with $\mathrm{Sp}_{\mathrm{cont}}(H_0)$. We know that this transfer is more efficient for special values of $\mathrm{Sp}_{\mathrm{cont}}(H_0)$, called resonances, for which the associated states have the behaviour of a bound state over an initial finite time interval before later having the behaviour of a scattering state. To display the resonances, we can use two techniques: the complex dilation method [20–25] or the optical potential model (also known as the complex absorbing potential method) [26–33]. Both methods transform H_0 into a non-self-adjoint Hamiltonian $\tilde{H}_0$.

The interaction of the molecule with a laser field is represented by the Hamiltonian

$$H(\vec{R}(t)) = \tilde{H}_0 + \mu E(t)\cos(\omega(t)t + \phi(t)), \tag{2}$$

where $\vec{R} = (E, \omega, \phi)$, E is the laser intensity, ω is the laser frequency, ϕ is the laser phase and μ is the electric dipole moment of the molecule. To treat the light–matter interaction, we use the adiabatic Floquet theory [2, 34] associated with the operator

$$H_F(\vec{R}, \theta) = \tilde{H}_0 + \mu E(\cos\theta\cos\phi - \sin\theta\sin\phi) - \mathrm{i}\hbar\omega_{\mathrm{eff}}\frac{\partial}{\partial\theta} \tag{3}$$

acting on the (r, θ)-dependent wavefunctions, with $\omega_{\mathrm{eff}}(t) = \dot{\omega}(t)t + \omega(t)$ (ω_{eff} replacing ω in the control parameters $\vec{R}$). It has been proved that the solution of the equation $\mathrm{i}\hbar\partial_t\psi(t,\theta) = H_F(\vec{R}(t),\theta)\psi(t,\theta)$ is such that $\psi(t, \theta = \omega(t)t)$ is a solution of the usual Schrödinger equation $\mathrm{i}\hbar\partial_t\psi(t,\omega(t)t) = H(\vec{R}(t))\psi(t,\omega(t)t)$ [34]. In fact the Floquet Hamiltonian $H_F(\vec{R},\theta)$ is the Hamiltonian of the system (molecule+field), where the state $\mathrm{e}^{\mathrm{i}n\theta}$ is an eigenvector of $\mathrm{i}\hbar\omega_{\mathrm{eff}}\partial_\theta$ ($n \in \mathbb{Z}$) and is the field state with n photons relative to the average

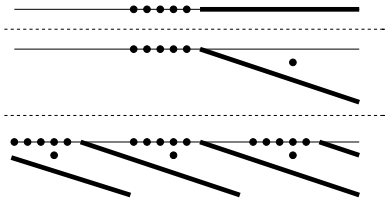

Figure 1. Illustration of the different deformations of the spectrum. From top to bottom: $\mathrm{Sp}(H_0)$, $\mathrm{Sp}(\tilde{H}_0)$ and $\mathrm{Sp}(H_F)$.

number of laser photons (see [35]). $\psi(t,\theta)$ is then the wavefunction of the molecule dressed by the field. $\mathrm{Sp}(H_F(\vec{R},\theta))$ is periodic and for $E=0$ we have $\mathrm{Sp}(H_F(0,\theta)) = \mathrm{Sp}(\tilde{H}_0)+\mathbb{Z}\hbar\omega$, see figure 1. From this point onward we assume that we use the optical potential model within the adiabatic Floquet treatment, and so can denote $H_F(\vec{R},\theta)$ simply by $H(\vec{R})$ without any confusion.

We suppose that at the initial time, the field is off. To summarize, the spectrum of $H_0 = H(\vec{R}(0))$ has three components: a real pure point part $\mathrm{Sp}_{\mathrm{bd}}(H_0)$ corresponding to the bound states, a complex pure point part $\mathrm{Sp}_{\mathrm{res}}(H_0)$ corresponding to the resonance states ($\mathrm{Sp}_{pp}(H_0) = \mathrm{Sp}_{\mathrm{bd}}(H_0)\cup\mathrm{Sp}_{\mathrm{res}}(H_0)$) and a (pseudo)-continuous part $\mathrm{Sp}_{\mathrm{cont}}(H_0)$ located in the lower complex half-plane and corresponding to the scattering states (resonance and scattering states are the two types of dissociative states, $\mathrm{Sp}_{\mathrm{diss}}(H_0) = \mathrm{Sp}_{\mathrm{res}}(H_0)\cup\mathrm{Sp}_{\mathrm{cont}}(H_0)$). The instantaneous spectrum of $H(\vec{R}(t))$ has a similar decomposition but during an evolution $t \mapsto \vec{R}(t)$, an eigenvalue can change its nature. Since we suppose that at $t=0$ the initial state is a bound state, there are three possible situations. First, the instantaneous eigenvector coming from the initial one can remain a bound state (the eigenvalue remains on the real axis at each instant); there is no dissociation and only transfers to other instantaneous bound states can occur. This situation corresponds to a weak field interaction and is analysed in the appendix. It is very similar to the N-level atom case studied by Yatsenko *et al* [1]. Second, the initial bound state can be distorted into a resonance state (the eigenvalue migrates into a lower complex half-plane), and transfers to other instantaneous resonance states can occur. This situation corresponds to a strong field interaction with slow variations of $\vec{R}$; it is analysed in section 3. Third, the initial bound state can be distorted into a resonance state until it becomes a scattering-like state (the eigenvalue migrates in the complex plane until approaching or entering the continuous spectrum). Transfers to instantaneous scattering states are then possible. This situation corresponds to a very strong field interaction or to a strong field interaction with fast variations of $\vec{R}$. It is analysed in section 4.

2.2. The dissociation processes

Dissociation can occur when the dynamical situation involves resonance or scattering states. It is very important to distinguish between two situations; as illustrated in [36], the dissociation via a resonance and the dissociation via a state associated with the continuum correspond to two different regimes. We can illustrate this difference by considering the photodissociation of the molecule H_2^+ with two different laser pulses of constant frequency $\omega = 0.296$ au (see figure 2) and with the ground bound state as an initial state. The wave packets corresponding to the projection of the wavefunction on the dissociative electronic states $^2\Sigma_u^+$ are drawn in figures 3 and 4. The dissociative wave packet can be interpreted as the wavefunction of the fragment issuing from the photodissociation (the proton escaping from the hydrogen atom located at $r=0$).

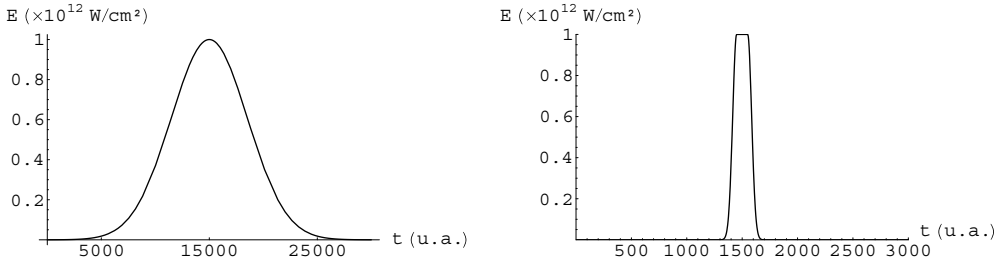

Figure 2. The left pulse is characterized by the envelope variation $E(t) = E_0\,\mathrm{e}^{-\frac{(t-t_1)^2}{\tau^2}}$ with $E_0 = 10^{12}\,\mathrm{W\,cm^{-2}}$, $t_1 = 15000$ au, $\tau = 5000$ au; the duration of the interaction is 30 000 au. This adiabatic interaction involves only the instantaneous resonance state issuing from the initial bound state. The right pulse is characterized by $E(t) = E_0\,\mathrm{e}^{-\frac{(t-t_1)^2}{\tau^2}}\ \forall t \in [0, t_1]$, $E(t) = E_0, \forall t \in [t_1, t_2]$ and $E(t) = E_0\,\mathrm{e}^{-\frac{(t-t_2)^2}{\tau^2}}\ \forall t > t_2$, with $E_0 = 10^{12}\,\mathrm{W\,cm^{-2}}, t_2 - t_1 = 100$ au, $\tau = 50$ au; the duration of the interaction is 3000 au. This second interaction involves scattering states.

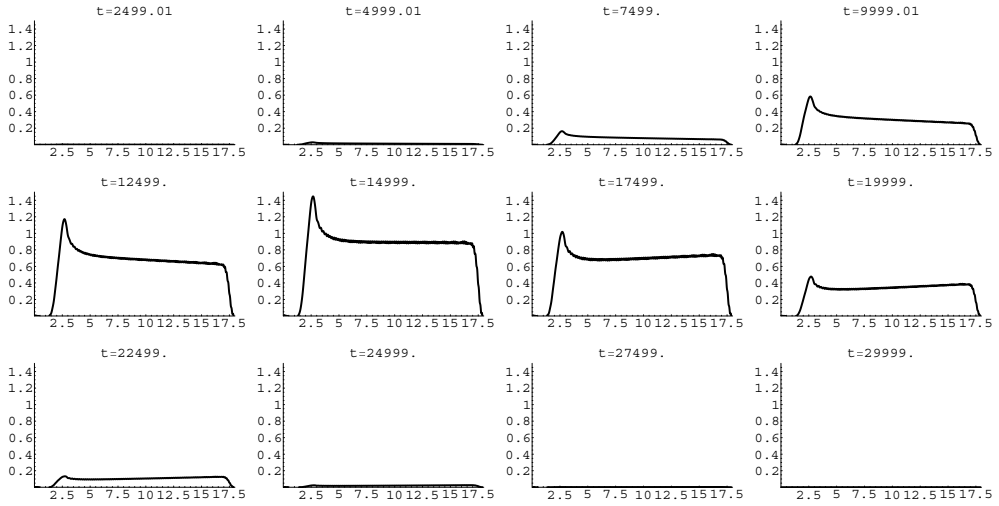

Figure 3. The dissociation wave packet of H_2^+ at 12 times for the dynamical process involving only a resonance. In each figure, the horizontal axis gives r in atomic units, and the vertical axis gives the wave packet amplitudes in arbitrary units. The optical potential starts at $r = 17$ au.

These figures show strong differences between the two regimes. In the case of a dissociation via a resonance, we see (figure 3) that the emitted fragment is delocalized with respect to r. We have a wave packet with a support covering $]0, r_0]$ ($[0, r_0]$ being the box used to model the system), with an amplitude increasing at the beginning of the dissociation and decreasing at the end (when the fragment absorbed asymptotically by the optical potential leaves the box). The duration of the dissociation, corresponding to the inverse of the imaginary part of the resonance, is then independent of the box length, and corresponds to the time needed for the fragment to pass through the molecular potential barrier by tunnelling. In contrast, the dissociation by scattering states (figure 4) shows a localized fragment (a wave packet with a short support) which moves from zero to the box wall. In this case, the duration of the dissociation (the inverse of the imaginary part of the quasi-continuum eigenvalues) depends on the box and corresponds to the time taken as the

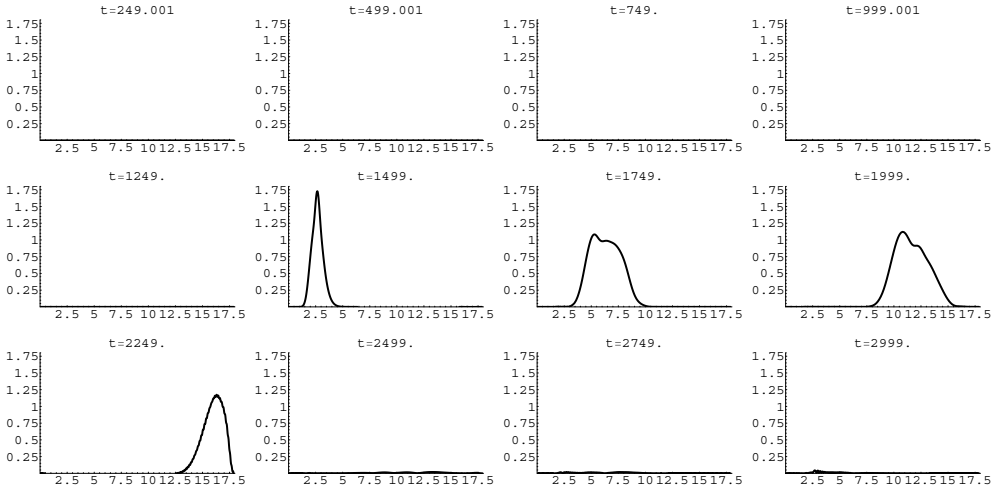

Figure 4. Same as figure 3 but for a dynamical process involving scattering states.

localized fragment covers the distance from 0 to r_0. When resonance and scattering states are simultaneously involved, as explained in [36], the scattering states are responsible for a transitional dissociative regime, whereas the resonance states are responsible for a permanent dissociative regime. For the interactions involving only a resonance it is not necessary to know the decomposition of the wavefunction in the $|r\rangle$-basis, because the dissociative process is completely delocalized. In this situation, we can reduce the analysis to involve a small active subspace (with dimension equal to 2 in the more simple cases). The first state of the active space represents the state issuing from the initial bound state and the second represents the state issuing from the resonance crossing the initial state. In the neighbourhood of the crossing, the dynamics can be represented by a 2×2 effective Hamiltonian matrix as explained in [11] for the case of a conservative system. Figures 3 and 4 illustrate the use of this low dimensional representation for dissociation via a resonance, in contrast with the case of dissociation via scattering states.

2.3. The adiabatic assumption and Berry phases

In order to analyse the population of the different eigenstates, we shall use an adiabatic formalism. The adiabatic approximation is a standard tool in quantum mechanics, and the well-known simple adiabatic theorem [37] appears as a basic concept of theoretical physics. Under certain conditions, this theorem states that the wavefunction remains in the same instantaneous eigenstate during the evolution so that no transition occurs. One of the required conditions is that the path $t \mapsto \vec{R}(t)$ does not approach a level crossing point in the manifold $\mathcal{M}$ of all configurations of $\vec{R}$, so that we have what we call the strong adiabatic regime. Other adiabatic theorems [38] state that the wavefunction remains projected into a space spanned by a small set of eigenvectors. Under these conditions, we can approach the level crossings within the small set and transitions between these states are possible. We refer to this situation as being in a quasi-adiabatic regime.

In 1984 Berry [12] proved that, within the adiabatic approximation, the wavefunction of a quantum dynamical system takes the form

$$\psi(t) = \mathrm{e}^{-\mathrm{i}\hbar^{-1}\int_0^t E_a(\vec{R}(t'))\,\mathrm{d}t' - \int_0^t \langle a,\vec{R}(t')|\partial_{t'}|a,\vec{R}(t')\rangle \mathrm{d}t'} |a,\vec{R}(t)\rangle, \tag{4}$$

where E_a is a nondegenerate instantaneous eigenvalue which is isolated from the rest of the Hamiltonian spectrum and which corresponds to the instantaneous eigenvector $|a, \vec{R}(t)\rangle$. $\vec{R}$ is a set of classical parameters used to model the time-dependent environment of the system. The set of all configurations of $\vec{R}$ is assumed to form a $\mathcal{C}^\infty$-manifold $\mathcal{M}$. The important feature is the presence of the extra phase term $\mathrm{e}^{-\int_0^t \langle a,\vec{R}(t')|\partial_{t'}|a,\vec{R}(t')\rangle \mathrm{d}t'} = \mathrm{e}^{-\int_{\mathcal{C}} \langle a,\vec{R}|\partial_\mu|a,\vec{R}\rangle \mathrm{d}R^\mu}$, called the Berry phase ($\mathcal{C}$ being the curve in $\mathcal{M}$ described by $t \mapsto \vec{R}(t)$). Simon [39] later found the mathematical structure which models the Berry phase phenomenon, namely a $U(1)$-principal bundle with the base space $\mathcal{M}$ and endowed with the gauge potential $A = \langle a, \vec{R}|\frac{\partial}{\partial R^\mu}|a, \vec{R}\rangle \, \mathrm{d}R^\mu$. Since the gauge group of the bundle formulation of the adiabatic theory is the same as the group of the bundle of electromagnetic field theory, we can identify the 1-form A with a magnetic potential in the virtual space $\mathcal{M}$. The bundle curvature $F = \mathrm{d}A$ can then be viewed as a magnetic field. It is known that if the studied eigenvalue E_a crosses another one at a point $\vec{R}_0 \in \mathcal{M}$, then F diverges at this point. A point divergence of a magnetic field must be interpreted as a magnetic monopole. Indeed, it is not difficult to prove (see, for example, [3]) that F and A satisfy the equations of the Dirac theory of magnetic monopoles [40–42]. The appearance of the Dirac monopole gauge structure in quantum dynamical systems in the adiabatic regime has been observed in several situations [4–11]. The topology of the adiabatic bundle and the adiabatic monopole picture are related by the fact that the magnetic charges of adiabatic monopoles are the first Chern classes of the adiabatic $U(1)$-bundle, the first Chern class being the non-triviality index of a bundle (see [3, 43]). It is possible to understand the adiabatic monopole properties and thence the topology of the adiabatic bundle by a local analysis in the neighbourhood of the crossings. This analysis involves a small effective Hamiltonian matrix [11], with an order equal to the number of crossing states. In the appendix we consider this case by considering, in place of $H(\vec{R})$, the 2×2-matrix $H^{\mathrm{eff}}(\vec{R})$ associated with a simple crossing. In the following section, we also use a 2×2 matrix $H^{\mathrm{eff}}(\vec{R})$ associated with a simple crossing between an eigenvalue issuing from a bound state energy and an eigenvalue issuing from a resonance. The delocalization observed for photodissociation via a resonance justifies the use of this low dimensional representation.

3. Topology of the processes involving resonance states

3.1. Illustrative model

We study an isolated crossing in the complex plane (and in the base manifold $\mathcal{M}$) of an eigenvalue issuing from a bound state and of an eigenvalue issuing from a shape resonance. To illustrate this situation, we propose the following model of a diatomic molecule. The molecule has two vibrational surfaces associated with two bound electronic states and a third vibrational surface associated with a pure dissociative electronic state (cf figure 5). A first permanent laser is used to couple the upper bound surface with the dissociative surface; the resulting adiabatic surfaces are drawn in figure 6. These surfaces have been obtained by application of the rotating wave approximation by supposing that the time of interaction in the resonance regime is much larger than the period of the laser light [45].

The structure of the lower adiabatic surface leads to a spectrum with continuum and shape resonances (see figure 7). A second laser subject to amplitude and frequency modulations couples the ground bound surface with the lower adiabatic surface, so that the coupling between bound states and shape resonances induces an isolated crossing of complex eigenvalues. Figure 8 shows the point of the plane $\mathcal{M} = (E, \omega)$ for which the eigenvalue issuing from the fifth bound state of the ground surface crosses the eigenvalue issuing from the third shape resonance of the lower adiabatic surface. Figure 9 shows in the complex plane the trajectories

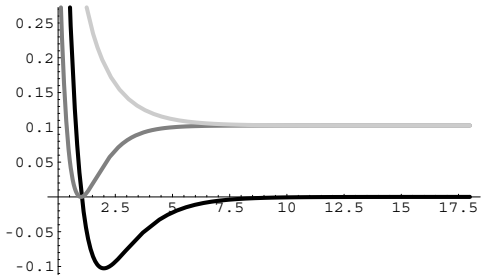

Figure 5. The three vibrational surfaces of our illustrative molecule: the surface associated with the ground bound electronic state is drawn in black, the surface associated with the excited bound electronic state is drawn in strong grey and the surface associated with the pure dissociative electronic state is drawn in light grey.

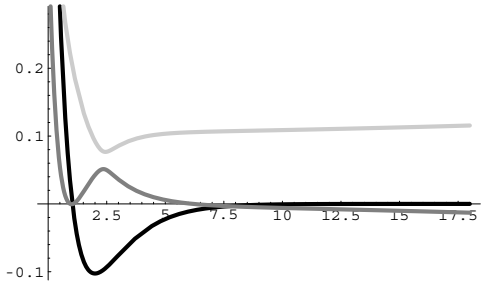

Figure 6. The lower bound surface (in black) and the two adiabatic surfaces (in grey) of the illustrative molecule when the first permanent laser is on.

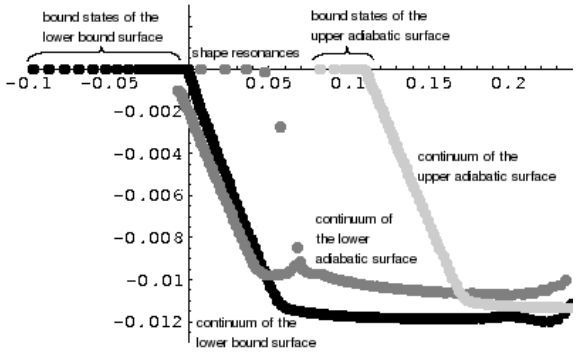

Figure 7. Vibrational spectrum in the complex plane of the illustrative molecule when the first permanent laser is on. The subspectrum associated with the ground bound surface is drawn in black, the subspectrum associated with the lower adiabatic surface is drawn in dark grey and the subspectrum associated with the upper adiabatic surface is drawn in light grey (the colours are the same as those in figure 6).

of the eigenvalues for two paths in the plane $\mathcal{M} = (E, \omega)$ (as shown in figure 8, the crossing is isolated in the space $\mathcal{M} = (E, \omega)$ so that each path in $\mathcal{M}$ passing through the crossing point induces an isolated crossing of eigenvalue trajectories in the complex plane). Since in the neighbourhood of the point crossing only two states are significantly involved in the adiabatic dynamics, we can study the crossing by using a 2×2 effective Hamiltonian matrix.

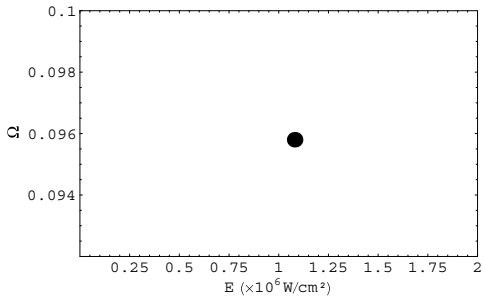

Figure 8. The plane $\mathcal{M} = (E, \omega)$ with the points which nullify the spectral distance in the complex plane between the eigenvalues issuing from the fifth bound state and from the third shape resonance. We see that that these two eigenvalues have an isolated crossing in $\mathcal{M}$.

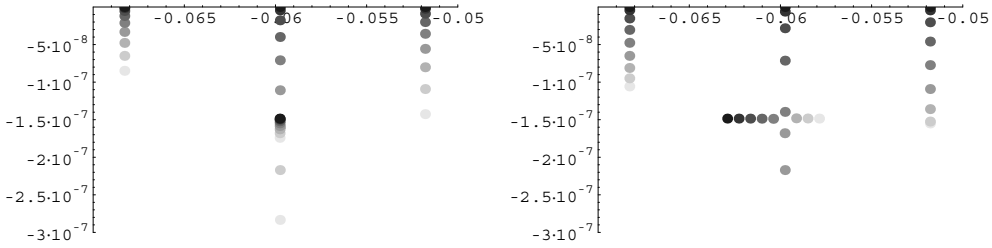

Figure 9. Left: trajectories in the complex plane of the eigenvalues issuing from the fourth, the fifth and the sixth bound states and from the third shape resonance, for a fixed frequency $\omega = 0.095\,85$ au with increasing values of E starting from 0 (in black) up to $18 \times 10^6\,\mathrm{W\,cm^{-2}}$ (in the darker light grey). Right: same as left but for a modulated frequency ω starting from 0.099 au up to 0.0933 au and a modulated amplitude E starting from 0 up to $25.2 \times 10^6\,\mathrm{W\,cm^{-2}}$ such that the straight line in $\mathcal{M}$ passes through the crossing point.

This illustrative example reveals the existence of isolated point crossings of two complex eigenvalues issuing from a bound state and from a shape resonance. The rest of this section will thus be devoted to a detailed analysis of such an adiabatic crossing with respect to the structure of the associated effective Hamiltonian.

3.2. Point resonance crossings

We now consider the situation where the initial bound state becomes an instantaneous resonance state under the influence of the field. In the neighbourhood of a crossing with another instantaneous state, the effective Hamiltonian takes the form

$$H^{\mathrm{eff}}(\vec{R}) = \frac{\hbar}{2}\begin{pmatrix} 0 & \Omega \\ \Omega & 2\Delta - \mathrm{i}\frac{\Gamma}{2} \end{pmatrix}. \tag{5}$$

We suppose that the resonance width Γ is constant ($\Gamma = 1$ au) and then can set $\vec{R} = (\Omega, \Delta)$. The effective Hamiltonian representation contains all the physical information because, as was seen in section 1, resonances induce a totally delocalized wave packet. It is then not necessary to have the $|r\rangle$-basis representation of the wavefunction.

The crossing of complex eigenvalues has been extensively studied in [44, 46] and the Berry phase phenomenon in this case has been studied in [47, 48].

We will extend the results (also see the appendix) and associate the dynamical effects with the topology of the adiabatic bundle, which is now a $\mathbb{C}^*$-principal bundle ($\mathbb{C}^*$ being the

group of non-zero complex numbers). The problem of the labelling of the states now takes a more complicated form. The eigenvalues are

$$E_{\pm}(\vec{R}) = \frac{\hbar}{2}\left(\Delta \pm \sqrt{\Omega^2 + \left(\Delta - \frac{\mathrm{i}}{4}\Gamma\right)^2} - \frac{\mathrm{i}}{4}\Gamma\right). \tag{6}$$

Using the notation of [46], we must distinguish $\mathcal{L}_R = \left\{\vec{R} \in \mathcal{M} \mid \Delta = 0, \Omega \in \left[-\frac{\Gamma}{4}, +\frac{\Gamma}{4}\right]\right\}$, the submanifold where the real parts of the resonances cross, from the submanifold $\mathcal{L}_I = \left\{\vec{R} \in \mathcal{M} | \Delta = 0, \Omega \in]-\infty, -\frac{\Gamma}{4}[\cup]\frac{\Gamma}{4}, +\infty[\right\}$, where the imaginary parts of the resonances (the reciprocal lifetimes) cross. The resonance crossings are in the intersection $\mathcal{L}_R \cap \mathcal{L}_I = \left\{\left(\pm\frac{\Gamma}{4}, 0\right)\right\}$.

When considering only the eigenvalues, without reference to the eigenvectors, there are two possible conventions for the labelling. The energy-ordering convention labels the states according to the real parts of the complex eigenvalues, and the lifetime-ordering convention labels the states according to the imaginary parts of the complex eigenvalues. The two conventions have a physical meaning: the first classifies the states according to their energies and the second classifies the states according to their dissipative characters. In a study of the dissociation, the second convention is probably more important. Moreover, we can also consider a state-ordering convention with a labelling according to the distances defined in the appendix with respect to the off-field states $|1\rangle = \binom{1}{0}$ and $|2\rangle = \binom{0}{1}$. As $|1\rangle$ is a bound state and $|2\rangle$ is a resonance state, we can suppose that the instantaneous state which is most close to $|1\rangle$ is the least dissipative state and the state which is most close to $|2\rangle$ is the most dissipative state. Indeed, the first-order perturbation treatment of the free Hamiltonian $\frac{\hbar}{2}\begin{pmatrix} 0 & 0 \\ 2\Delta & -\frac{\mathrm{i}}{2}\Gamma \end{pmatrix}$ by $\frac{\hbar}{2}\begin{pmatrix} 0 & \Omega \\ \Omega & 0 \end{pmatrix}$ leads to

$$E_1(\vec{R}) = 0 + \mathcal{O}(\Omega^2) \tag{7}$$

$$|1, \vec{R}\rangle = |1\rangle - \frac{\Omega}{2\Delta - \frac{\mathrm{i}}{2}\Gamma}|2\rangle + \mathcal{O}(\Omega^2) \tag{8}$$

$$E_2(\vec{R}) = \frac{\hbar}{2}\left(2\Delta - \frac{\mathrm{i}}{2}\Gamma\right) + \mathcal{O}(\Omega^2) \tag{9}$$

$$|2, \vec{R}\rangle = |2\rangle + \frac{\Omega}{2\Delta - \frac{\mathrm{i}}{2}\Gamma}|1\rangle + \mathcal{O}(\Omega^2). \tag{10}$$

We would then conclude that the state-ordering convention is identical to the lifetime-ordering convention. This assumption is confirmed by numerical tests. The state-ordering convention then appears to be less artificial in the resonance case than in the bound case treated in the appendix. Moreover, figures 10 and 11 show that the real parts of the eigenvalues are continuous in the energy-ordering convention, whereas they present a strong discontinuity on $\mathcal{L}_I$ in the state-ordering convention. Conversely the imaginary parts (the reciprocal lifetimes) are continuous in the state-ordering convention, whereas they present a strong discontinuity on $\mathcal{L}_R$ in the energy-ordering convention. In contrast to the bound case, where we can arbitrarily choose the line separating the two charts, this line must be $\mathcal{L}_R \cup \mathcal{L}_I$ in the resonance case because of the two discontinuities (in the real and the imaginary parts).

The magnetic field distribution is found to be as represented in figure 12. We see that, in addition to the monopoles at $\mathcal{L}_R \cap \mathcal{L}_I$, the effective magnetic field makes the submanifold $\mathcal{L}_R$ appear in the energy-ordering convention, whereas in the state-ordering convention it gives rise to the submanifold $\mathcal{L}_I$.

In the bound state case, we have identified two different types of adiabatic passages: a rapid passage consisting of a state swap in the two conventions (figure A5), and a

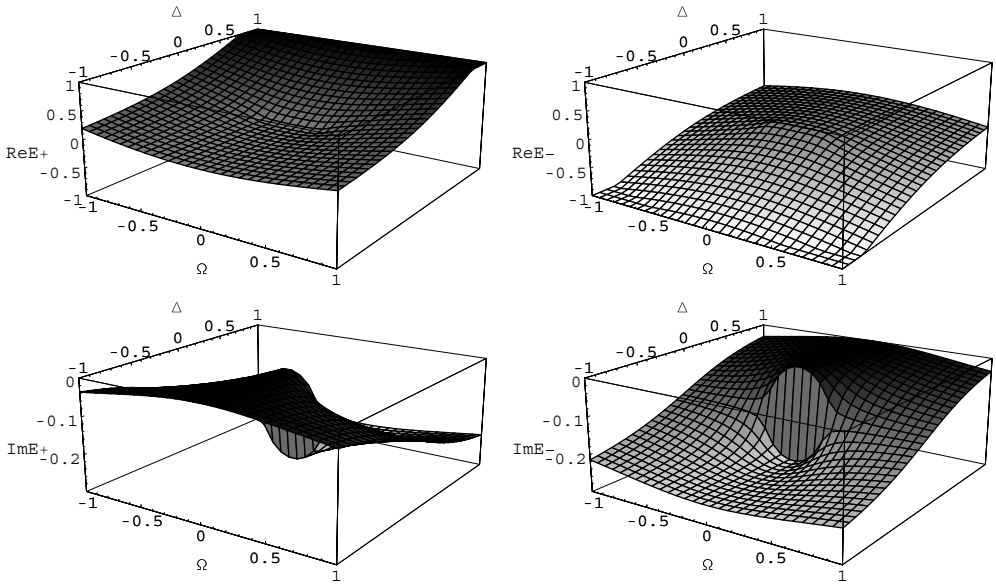

Figure 10. Real and imaginary parts of the eigenvalues in the energy-ordering convention as a function of Ω and Δ for a resonance crossing.

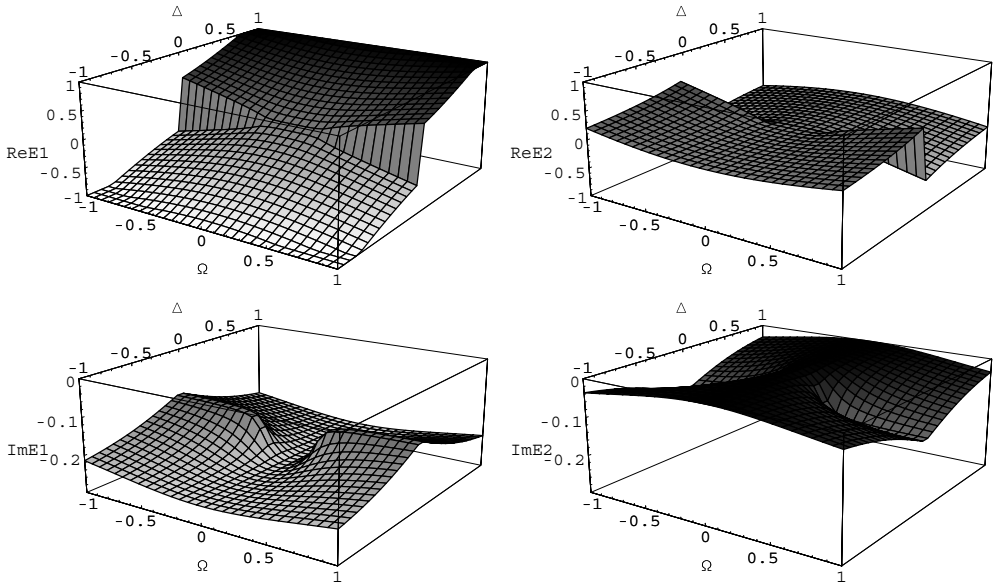

Figure 11. Real and imaginary parts of the eigenvalues in the state-ordering convention (the lifetime-ordering convention) as a function of Ω and Δ for a resonance crossing.

direct chirping effect consisting of a state swap in the state-ordering convention with no swap in the energy-ordering convention (figure A6). In the resonance case, these two effects are replaced by two others. First, the paths which cross $\mathcal{L}_R$ induce a dynamics with population transfers in terms of the energy but such that the wavefunction remains that of the less dissipative state. We then have a weak dissipative dynamics and a state

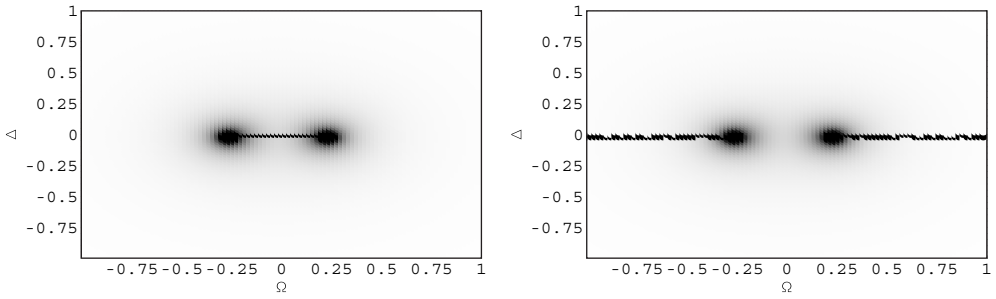

Figure 12. The plane (Ω, Δ) for a resonance crossing, with the monopole magnetic field (in black), for the energy-ordering convention (left) and for the state-ordering convention (right).

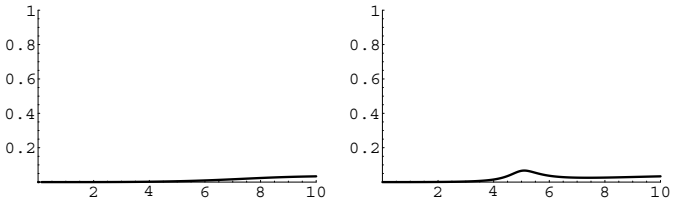

Figure 13. Dissipation rate (left) and probability of dissociation (right) for a dynamical trajectory crossing $\mathcal{L}_R$.

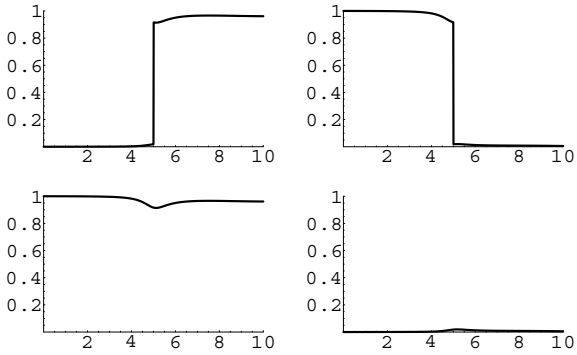

Figure 14. Up: instantaneous occupation probabilities $|\langle +*, \vec{R}(t)|\psi(t)\rangle|^2$ (left) and $|\langle -*, \vec{R}(t)|\psi(t)\rangle|^2$ (right). Down: instantaneous occupation probabilities $|\langle 1*, \vec{R}(t)|\psi(t)\rangle|^2$ (left) and $|\langle 2*, \vec{R}(t)|\psi(t)\rangle|^2$ (right), for a dynamical trajectory crossing $\mathcal{L}_R$.

swap in the energy-ordering convention (at the very instant that the path crosses $\mathcal{L}_R$) and without a swap in the state-ordering convention. These effects for the path $t \mapsto \vec{R}(t) = (\Omega(t) = 0.1\sin(\pi t/10), \Delta(t) = 1.1\cos(\pi t/10))$ are presented in figures 13 and 14. Second, the paths which cross $\mathcal{L}_I$ induce no population transfer from the energy viewpoint, but induce population transfers from the lifetime viewpoint. We then have a strong dissipative dynamics and a state swap for the state-ordering convention at the moment when the path crosses $\mathcal{L}_I$, with conversely no swap in the energy-ordering convention. These effects are illustrated with the path $t \mapsto \vec{R}(t) = (\Omega(t) = 1\sin(\pi t/15), \Delta(t) = 1.1\cos(\pi t/15))$ in figures 15 and 16. For a dynamical trajectory approaching a monopole, these effects are accompanied by non-adiabatic transitions which transfer quantum flux in terms of the energy and of the dissipative character. The energy-order labelling must be used to exhibit the population transfer effects

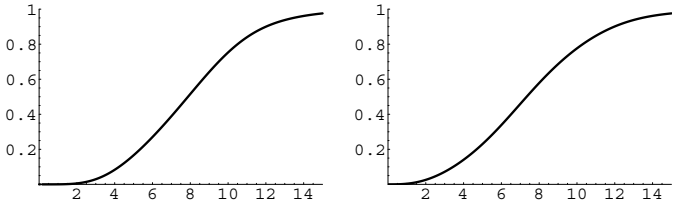

Figure 15. Dissipation rate (left) and probability of dissociation (right) for a dynamical trajectory crossing $\mathcal{L}_I$.

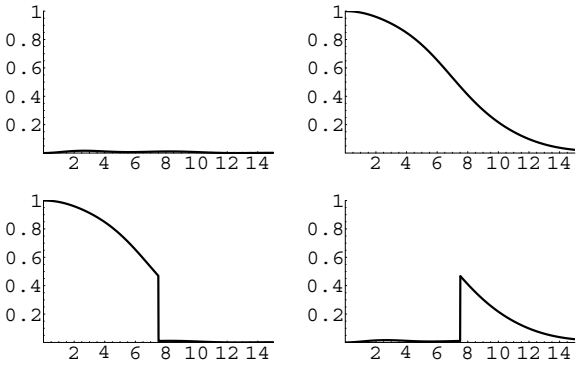

Figure 16. Up: instantaneous occupation probabilities $|\langle +*, \vec{R}(t)|\psi(t)\rangle|^2$ (left) and $|\langle -*, \vec{R}(t)|\psi(t)\rangle|^2$ (right). Down: instantaneous occupation probabilities $|\langle 1*, \vec{R}(t)|\psi(t)\rangle|^2$ (left) and $|\langle 2*, \vec{R}(t)|\psi(t)\rangle|^2$ (right), for a dynamical trajectory crossing $\mathcal{L}_I$.

in the same manner as for the conservative case (the rapid passages or the non-adiabatic transitions between two states with different energies). The dissipative analogue to the non-dissipative rapid passage is the passage through a monopole at $\mathcal{L}_R \cap \mathcal{L}_I$, which simultaneously induces population transfers from the viewpoint of the energy and of the dissipative character. The state-ordering labelling must be used to exhibit a passage between a weakly and a strongly dissipative state. We note that direct chirping is the non-dissipative analogue of this effect.

3.3. One-dimensional resonance crossings

The choice of other control parameters necessarily leads to situations which are different from those treated in the previous paragraph. First, suppose that we fix the detuning (the laser frequency) and that we impose a phase modulation. The effective Hamiltonian is then

$$H^{\text{eff}}(\vec{R}) = \frac{\hbar}{2}\begin{pmatrix} 0 & x - \mathrm{i}y \\ x + \mathrm{i}y & 2\Delta - \frac{\mathrm{i}}{2}\Gamma \end{pmatrix}, \tag{11}$$

where $x - \mathrm{i}y = \Omega\,\mathrm{e}^{\mathrm{i}\phi}$, Δ and Γ being constants (we choose $\Delta = 0$ and $\Gamma = \sqrt{2}$ without loss of generality). In this case, the eigenvalues are

$$E_{\pm}(\vec{R}) = \frac{\hbar}{2}\left(-\frac{\mathrm{i}}{4}\Gamma \pm \sqrt{x^2 + y^2 - \frac{\Gamma^2}{16}}\right). \tag{12}$$

The eigenvalue crossing is then represented by a circle $\mathcal{S}$ centred on zero with a radius equal to $\frac{\Gamma}{4}$. The real parts of the resonances cross at the interior of $\mathcal{S}$, whereas the imaginary parts cross

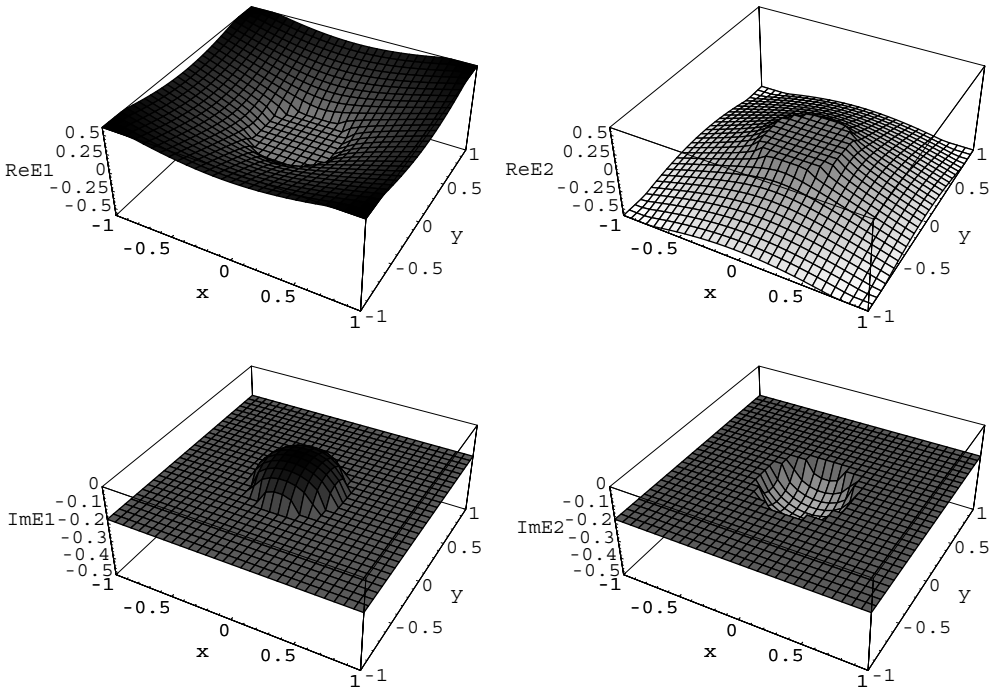

Figure 17. Real and imaginary parts of the eigenvalues as a function of $x = \Omega\cos\phi$ and $y = \Omega\sin\phi$ for a resonance crossing with phase modulations and constant frequency.

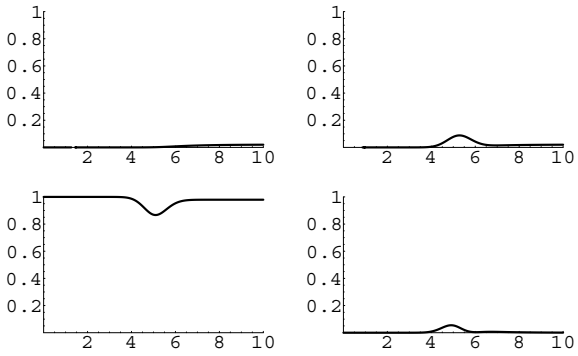

Figure 18. Up: dissipation rate (left) and probability of dissociation (right) for the dynamics inside the circle for a resonance crossing with phase drift. Down: instantaneous occupation probabilities $|\langle 1*, \tilde{R}(t)|\psi(t)\rangle|^2$ (left) and $|\langle 2*, \tilde{R}(t)|\psi(t)\rangle|^2$ (right). We observe a small non-adiabatic transfer.

at the exterior (see figure 17). It is then impossible to adopt the energy-ordering convention in the interior of the circle because the energy is degenerate, and it is impossible to adopt the state-ordering convention outside the circle because the eigenvectors are equidistant of the off-field states. The only convention able to describe the fibre bundle topology is that associated with two charts: one corresponding to the interior of the circle (where we adopt the state-ordering labelling) and one corresponding to the exterior of the circle (where we adopt the energy-ordering convention).

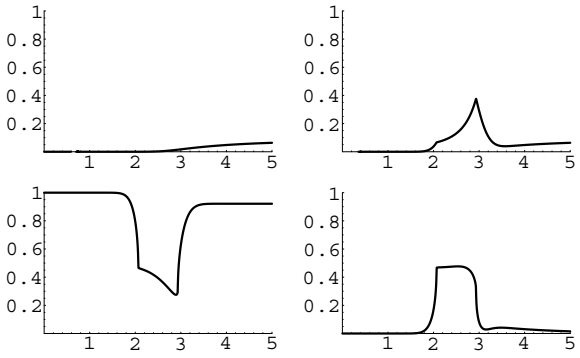

Figure 19. Up: dissipation rate (left) and probability of dissociation (right) for a dynamical trajectory crossing the circle $\mathcal{S}$, for a resonance crossing with phase drift. Down: instantaneous occupation probabilities $|\langle 1*, \tilde{R}(t)|\psi(t)\rangle|^2$ (left) and $|\langle 2*, \tilde{R}(t)|\psi(t)\rangle|^2$ (right). The population inversions are not sudden because of small non-adiabatic transitions occurring at the approach to the circle.

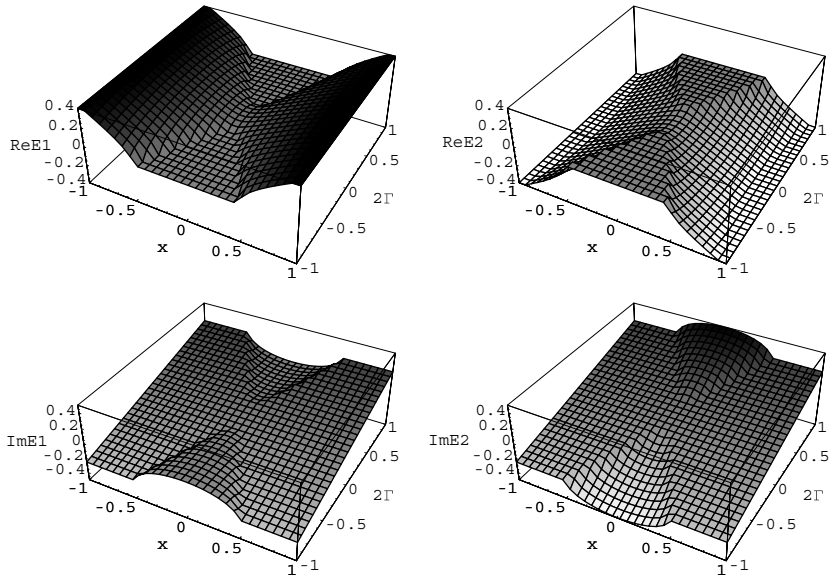

Figure 20. Real and imaginary parts of the eigenvalues as a function of $x = \Omega\cos\phi$ and Γ for a resonance crossing with variations of Γ.

Let the dynamics be induced by a laser pulse $\Omega(t) = \Omega_0\, \mathrm{e}^{-(t-t_0)^2/\tau}$ with a phase drift proportional to the time, $\phi(t) = \frac{\pi}{2} + \alpha t$. For $\Omega_0 = 0.2$ au, $t_0 = 5$ au and $\alpha = \frac{\pi}{5}$ au, the path is a little loop starting from zero and remaining inside the circle. In this case, the dynamics is weakly dissipative and no population transfer occurs (see figure 18). For $\Omega_0 = 0.75$ the loop crosses the circle, the dissipation is stronger and population transfers occur at each passage by the circle (figure 19). Similar results, with $\mathcal{S}$ a hyperbola rather than a circle, are obtained by fixing y and by varying Γ (see figure 20). The representation in terms of the magnetic field distribution allows us to visualize this situation just as in the previous case (figure 21).

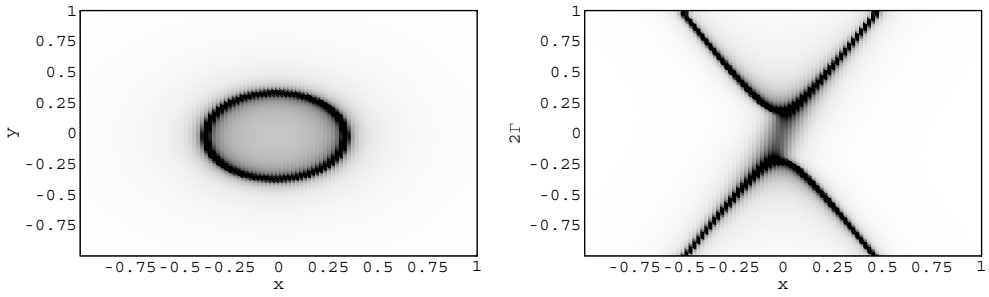

Figure 21. The monopole magnetic field (in black), for a resonance crossing in the planes $(x = \Omega\cos\phi, y = \Omega\sin\phi)$ (left) and (x, Γ) (right).

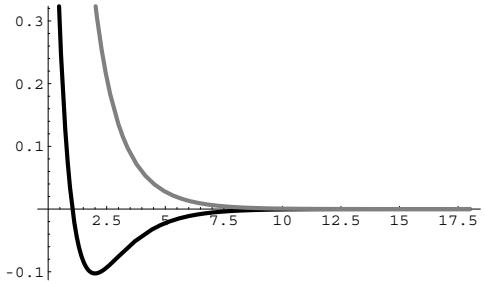

Figure 22. Vibrational surfaces modelling the molecule H_2^+; the surface associated with $^2\Sigma_g^+$ is drawn in black and the surface associated with $^2\Sigma_u^+$ is drawn in grey.

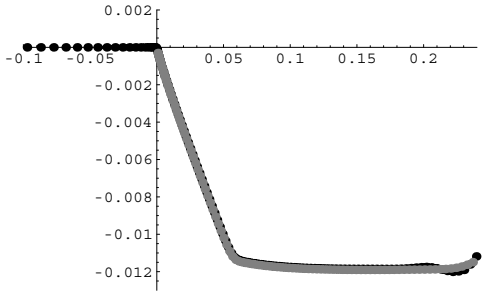

Figure 23. Spectrum of H_2^+ in the complex plane; the subspectrum associated with $^2\Sigma_g^+$ is drawn in black and the subspectrum associated with $^2\Sigma_u^+$ is drawn in grey (in agreement with figure 22). We note that the continua of $^2\Sigma_g^+$ and of $^2\Sigma_u^+$ are confused.

4. Topology of the processes involving the continuum

In this section, we treat the case of a resonance which approaches the continuum or which has non-adiabatic couplings with the continuum. Within the optical potential model, the continuum is discretized and is replaced by a sequence of eigenvalues. The coupling between the continuum and the instantaneous resonance issuing from the initial state is then treated as couplings between the instantaneous resonance issuing from the inital state and several instantaneous pseudo-resonances representing the continuum in the model (the eigenvalues of the pseudo-continuum). We can then apply the results of the previous section. As an example, we have considered the case of the molecule H_2^+, modelled with two vibrational surfaces (figure 22), and which presents the spectrum drawn in figure 23. We have drawn the effective

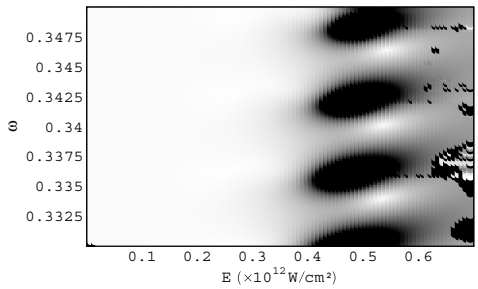

Figure 24. The monopole magnetic field (in black) for the resonance issuing from the second bound state of H_2^+, as a function of (E, ω). We have adopted here the state-ordering labelling which is the only consistent convention involving the scattering states. The structures appearing for $E > 0.6$ are numerical artifacts caused by difficulties with the convergence of the diagonalization program for the matrix representing the Hamiltonian of H_2^+ in very strong fields.

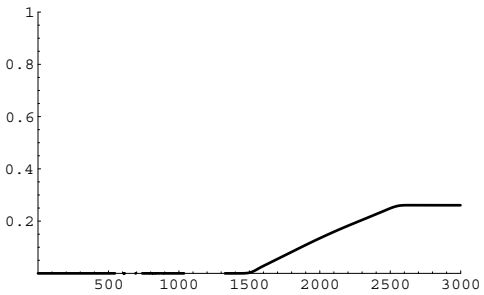

Figure 25. The accumulated outgoing quantum flux for a non-adiabatic dynamical process starting from the second bound state of H_2^+.

magnetic field distribution (figure 24) for the resonance issuing from the second bound state of the molecule H_2^+ interacting with a laser field. The different crossings between the eigenvalues of the pseudo-continuum and the resonance induce an image of the quasi-continuum in $\mathcal{M}$ (a sequence of magnetic monopoles that we can call a seam in accordance with the expression used in the literature in another context [49–51]). We can then make a correspondence between the different fields and the associated quasi-continuum states; the order in the sequence of the monopoles with respect to ω is the order of the energies of the associated states. Note that it is important to know, as a function of $\vec{R}$, with which scattering states the resonance is coupled, because the energies of these states determine the speed of the wave packet emitted on the dissociation plateau: consider, for example, the laser pulse $E(t) = 0.1\,\mathrm{e}^{-((t-1000)/50)^2}$ if $t < 1000$, $E(t) = 0.1$ if $t \in [1000, 2000]$ and $E(t) = 0.1\,\mathrm{e}^{-((t-2000)/20)^2}$ if $t > 2000$. Starting from the second bound state of H_2^+, we have drawn the outgoing quantum flux (figure 25) and the dissociation wave packet (figure 26). The energies of the scattering states which are coupled with the instantaneous resonance determine the speed of the dissociation wave packet front (see figure 26), and thus the duration of the transitional regime of the dissociation. They also determine the delay of the outgoing quantum flux with respect to the case where no scattering states are involved. The outgoing quantum flux (figure 25) starts at a later time when scattering states are involved than when only a resonance state is involved, see [36].

It is interesting to consider the limiting case of an exact description of the continuum. At this limit a continuous seam of monopoles should appear in $\mathcal{M}$, and it is evident that this line is

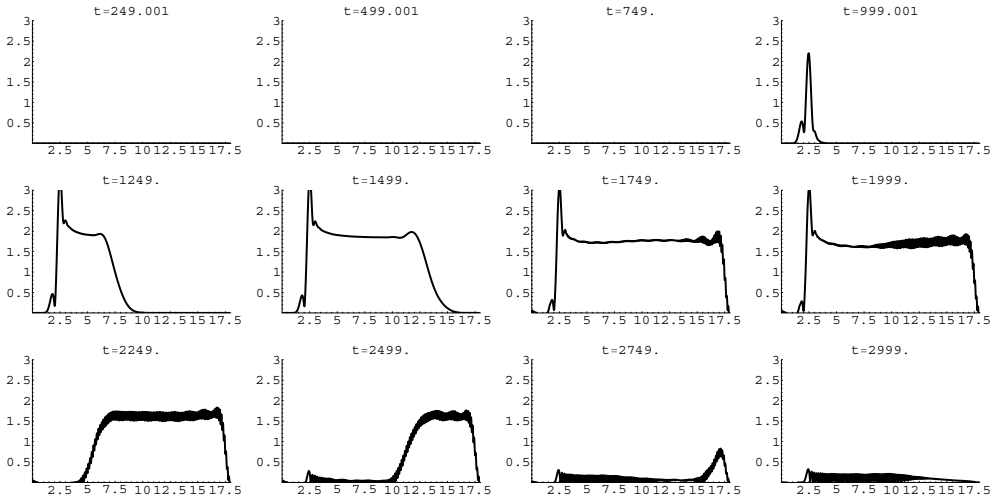

Figure 26. The dissociation wave packet of H_2^+ at 12 times for the dynamical process involving non-adiabatic transfers to scattering states. In each figure, the horizontal axis is r in atomic units and the vertical axis is the wave packet amplitude in arbitrary units.

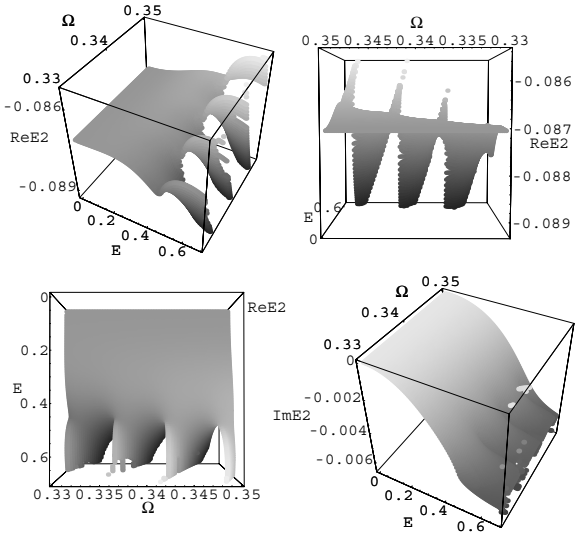

Figure 27. Real part of the eigenvalue issuing from the second bound state of H_2^+ as a function of (E, ω) for different views, except for the left lower figure which represents the imaginary part.

also the neighbourhood of charts describing the topology of the adiabatic bundle. Indeed, this line corresponds to the continuum embedding of the resonance and so to a boundary between two relaxation schemes: to the left of this seam the state issuing from the inital bound state is a resonance state, and to the right it is a scattering state. The monopole seams (and thus the chart system) and the resulting magnetic field are associated with a transition between dissipative regimes. The non-adiabatic transitions induce the passage from the permanent dissociative regime (produced only by the resonance state issuing from the initial bound state) to the transitional dissociative regime (generated simultaneously by the scattering states) (see [36] for more details).

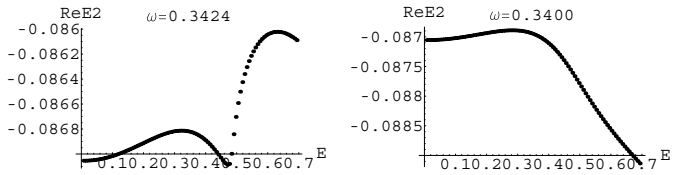

Figure 28. Real part of the eigenvalue issuing from the second bound state of H_2^+ as a function of E, for a frequency corresponding to a monopole (left) and for a frequency corresponding to a hole (right).

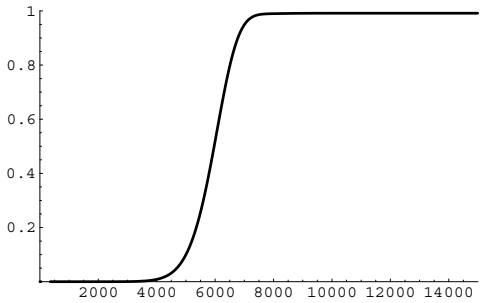

Figure 29. The accumulated outgoing quantum flux for the adiabatic dynamical process approaching the continuum and starting from the second bound state of H_2^+.

Nevertheless, we note that figure 24 reveals a difficulty. The discretization process introduces holes in the transition line which can induce errors in the description of the system. These errors are made clear by drawing the surfaces associated with the resonances (figure 27). A direct consequence is the presence of strong discontinuities in the real part of the eigenvalue: it takes higher values at the positions of the monopoles and lower values at the position of the holes produced by the discretization (figure 28). These discontinuities are numerical artifacts; fortunately, they do not have a drastic effect on the final results. Indeed, to be embedded in the continuum the resonance needs to be located very low in the complex plane and thus involve a strong dissipation. From the viewpoint of the wavefunction, the dissipation is complete before the continuum can be reached. Consider, for example, the laser pulse $E(t) = 0.4\,\mathrm{e}^{-((t-7500)/2500)^2}$, with $\omega = 0.342$. This is a limit case of a strong adiabatic regime, for which the wavefunction remains that of the instantaneous resonance and also the end of the dissipation is as late as possible. Nevertheless, figure 29 shows that the dissipation is complete at the instant $t = 7500$, corresponding to the point of the path which is the closest to the continuum.

5. Conclusion

The quantum effects appearing within the context of adiabatic dynamics can be considered as manifestations of the topology of the adiabatic bundle. The adiabatic passage (a sudden transition occurring on passing through a degeneracy point of the eigenvalues) studied by Yatsenko *et al* [1] is associated with virtual magnetic monopoles, and thus with the adiabatic bundle topology. We have seen in this paper that the direct chirping effect is also a manifestation of this topology. The passage through a chart transition region (in practice reduced to a line for the two-dimensional cases) is responsible for the direct chirping effect. We have seen that this problem of identifying the topology is intimately related to the problem of state labelling.

Table 1. Relations between some quantum dynamical effects and different methods of interpretation for the general case.

Surfaces topology	Bundle topology/ magnetic monopole picture	Dynamical effects
Crossings of the real parts	Transition lines $\mathcal{L}_R$	Population transfers from the viewpoint of the energies
Crossings of the imaginary parts	Transition lines $\mathcal{L}_I$ (arbitrary in the conservative case)	Passages from weak to strong (or conversely) permanent dissociative regimes (direct chirping in the conservative case)
Eigenlevel crossings	Magnetic monopoles	Population transfer and swap of permanent dissociative regimes
Continuum embedding of resonances	Continuous monopoles seams	Passages from permanent to transitional dissociative regimes
Contact order of the crossings	Distribution of the monopole magnetic fields (magnetic charge)	Amplitudes of the non-adiabatic couplings \hline

This analysis allows us to extend the results of Yatsenko *et al* to the cases of three-dimensional conservative systems and to two-dimensional and three-dimensional dissipative systems. In the dissipative case, we have seen that the problem is more complicated and we have pointed out the complementary roles of the two labelling conventions. The energy-ordering labelling is associated with the adiabatic passage from the viewpoint of the energy, and the state-ordering labelling is associated with the passage between different dissociative regimes (from a weak to a strong dissipative regime and conversely for the coupling between two resonance states, and from a permanent to a transitional regime for the coupling of a resonance state with scattering states). These results are summarized in table 1.

Moreover, the method of visualization of the topology, by drawing the effective magnetic field based on an n-dimensional graph for n control parameters, should be more practicable for complex situations than the representation using the eigensurfaces. In this paper, in order to explain the meaning of the figures, we have also drawn the eigensurfaces.

Acknowledgments

This work is supported by grants from *Agence Nationale de la Recherche* (CoMoC project).

Appendix. Topology of the processes involving bound states

We consider the situation in which only instantaneous bound states participate. In the neighbourhood of the crossing of the initial state with another instantaneous bound state, the effective dressed Hamiltonian takes the form

$$H^{\text{eff}}(\vec{R}) = \frac{\hbar}{2}\begin{pmatrix} 0 & \Omega\,\mathrm{e}^{\mathrm{i}\phi} \\ \Omega\,\mathrm{e}^{-\mathrm{i}\phi} & 2\Delta \end{pmatrix}. \tag{A.1}$$

Here $\vec{R} = (\Omega, \Delta, \phi)$ where $\Omega = |\langle 1|\mu E|2\rangle|$ and $\Delta = E_2 - E_1 - \hbar\omega$. $|1\rangle = \binom{1}{0}$ is the initial bound state, E_1 being its eigenvalue, and $|2\rangle = \binom{0}{1}$ is the other bound state when the laser is off, E_2 being its eigenvalue. In order to simplify the analysis we restrict our attention to the case $\phi = 0$, because ϕ does not play an important role in the following discussion.

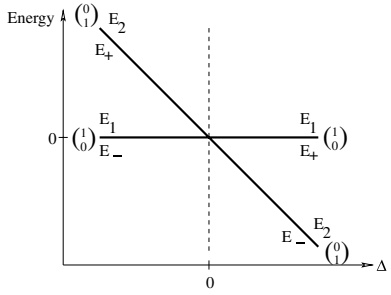

Figure A1. The two eigenvalues as a function of Δ, with the convention (E_+, E_-) which follows the energy order and with the convention (E_1, E_2) which follows the eigenvectors $|1\rangle = \binom{1}{0}$ and $|2\rangle = \binom{0}{1}$.

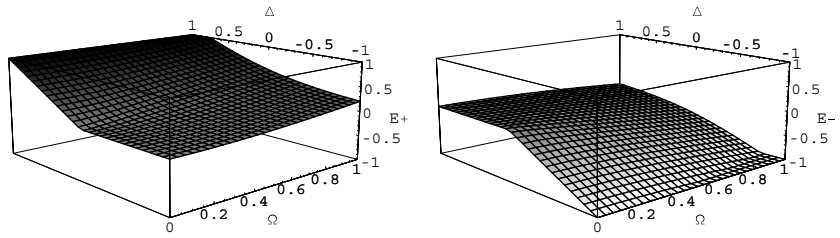

Figure A2. Energy surfaces in the energy-order convention as a function of Ω and Δ for a bound state crossing.

A.1. Eigenvalue labelling

We consider the 'off-field' dynamical system, with $\Omega = 0$. We now have a single control parameter Δ. The Hamiltonian $H^{\text{eff}} = \begin{pmatrix} 0 & 0 \\ 0 & \hbar\Delta \end{pmatrix}$ has two eigenvalues which cross at $\Delta = 0$. For $\Delta < 0$ and $\Delta > 0$, it is possible to follow continuously the eigenvalues and their eigenvectors, but we have two possible conventions for the passage through $\Delta = 0$. One follows the energy order of the eigenvalues and the other follows the eigenvectors, as we can see in figure A1. For $\Omega > 0$, we can follow continuously the eigenvalues at each $\vec{R}$:

$$E_\pm(\vec{R}) = \frac{\hbar}{2}(\Delta \pm \sqrt{\Omega^2 + \Delta^2}). \tag{A.2}$$

This continuous following is associated with the convention which follows the energy order (see figure A2). This convention is arbitrary; in particular, we observe that

$$\lim_{\Omega\to 0} |+, \vec{R}\rangle = \begin{cases} \binom{0}{1} & \text{if} \quad \Delta \geqslant 0 \\ \binom{1}{0} & \text{if} \quad \Delta < 0 \end{cases} \tag{A.3}$$

$$\lim_{\Omega\to 0} |-, \vec{R}\rangle = \begin{cases} \binom{1}{0} & \text{if} \quad \Delta \geqslant 0 \\ \binom{0}{1} & \text{if} \quad \Delta < 0. \end{cases} \tag{A.4}$$

The energy-order convention is then not consistent with the following off-field eigenvector. There is an infinity of possible conventions which are consistent with this following off-field eigenvector: for example, we can draw an arbitrary line separating in two regions the plane (Ω, Δ) passing by $(0, 0)$ (the level crossing) and then swap the labels with respect to the energy-order convention at the passage through this line. However, there does exist a

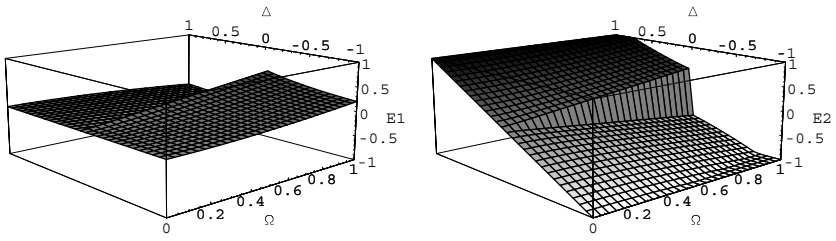

Figure 3. Energy surfaces in the state-ordering convention as a function of Ω and Δ, for a bound state crossing.

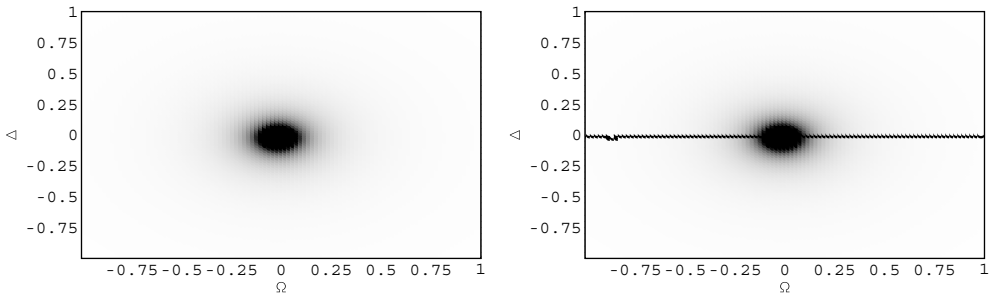

Figure A4. The plane (Ω, Δ) for bound state crossing, with the monopole magnetic field (in black), for the energy-ordering convention (left) and for the state-ordering convention (right). We have extended the domain to $\Omega < 0$ in order to have a symmetric figure.

particular convention which is physically significant. This convention is one which assigns label 1 to the state which is closer to the initial bound state and label 2 to the other state. Two states are defined to be close if their scalar product is large. This convention thus assigns the labels 1 and 2 so as to satisfy the inequality

$$|\langle 1|1, \vec{R}\rangle| \times |\langle 2|2, \vec{R}\rangle| > |\langle 2|1, \vec{R}\rangle| \times |\langle 1|2, \vec{R}\rangle|. \tag{A.5}$$

This state-ordering convention thus has a strongly relevant physical meaning but, like other conventions consistent with the following off-field state, it induces a discontinuity in the energy surfaces (see figure 3). The recognition of the state which is closer to an off-field state is physically important; the interpretation of an instantaneous eigenstate is not clear (since it corresponds to a non-equilibrium state), whereas the physical meaning of the off-field state is clear.

It is possible to make the topology of the adiabatic bundle play a role in numerical calculations by considering the adiabatic magnetic field associated with the magnetic monopole representing the crossing. In the energy-ordering convention only the magnetic monopole appears, whereas in the state-ordering convention the chart intersection also appears (see figure A4).

A.2. Interpretation of dynamical processes

In this paragraph, we show that the usual dynamical processes of population transfer can be interpreted by using the framework of the adiabatic bundle topology and by looking at the results show in figure A4. These interpretations can be compared with the alternative ones given in [1, 2].

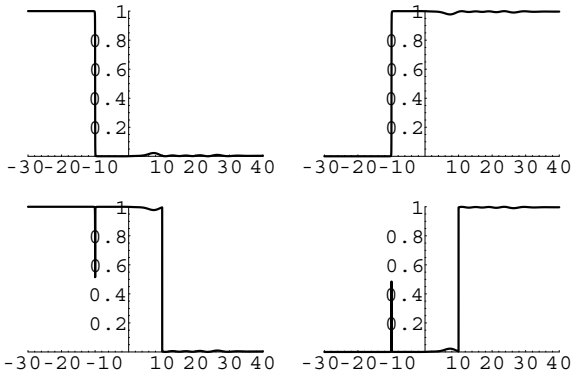

Figure A5. Up: instantaneous occupation probabilities $|\langle +, \vec{R}(t)|\psi(t)\rangle|^2$ (left) and $|\langle -, \vec{R}(t)|\psi(t)\rangle|^2$ (right), Down: instantaneous occupation probabilities $|\langle 1, \vec{R}(t)|\psi(t)\rangle|^2$ (left) and $|\langle 2, \vec{R}(t)|\psi(t)\rangle|^2$ (right), for the Stark chirped adiabatic passage dynamics. The peaks appearing at time $t \simeq -10$ au for the state-ordering convention are numerical artifact due to the degenerate character of this convention at the precise position of the crossing.

The first dynamical process studied corresponds to the Stark chirped adiabatic passage effect and is characterized by the path $t \mapsto \vec{R}(t) = \left(\Omega(t) = 1.5\,\mathrm{e}^{-(t-15)^2/10^2}, \Delta(t) = -1 + 2\,\mathrm{e}^{-t^2/12^2}\right)$. This path is followed sufficiently slowly to be in a strong adiabatic regime, except at time $t \simeq -10$ au, when the path passes through the eigenvalue crossing (see figure A5). We see that in the energy-ordering convention, the transition occurs when the path encounters the monopole (the eigenvalue crossing). In the state-ordering convention, the transition occurs when the path crosses the line separating the two regions of $\mathcal{M}$ (see figure A4). In this case, the representation of the wavefunction in the state-ordering convention could appear to be artificial. Nevertheless, we see in section 3 that for the description of other effects (or in the complex case) it is physically relevant.

We now consider the dynamics of the direct chirping effect, $t \mapsto \vec{R}(t) = (\Omega(t) = 1.1\sin(\pi t/10), \Delta(t) = 1.1\cos(\pi t/10))$. This dynamical process is also sufficiently slow to be in a strong adiabatic regime; thus no transition occurs. If we start with state $|-, \vec{R}(0)\rangle$, we finish with $|-, \vec{R}(10)\rangle$. This fact appears clearly within the energy-ordering convention, where the wavefunction is projected only on $|-, \vec{R}\rangle$ (see figure A6). However we have $|+, \vec{R}(0)\rangle = \binom{0}{1}$ and $|-, \vec{R}(10)\rangle = \binom{1}{0}$, whereas during the direct chirping process no transition occurs, because the path does not pass close by the monopole. In fact, the transition from one off-field state to the other between the inital and the final time is due to the permutation $\left(\begin{smallmatrix}0 & 1\\ 1 & 0\end{smallmatrix}\right)$ associated with the line separating $\mathcal{M}$ into two regions. It is the passage from one region to another which induces the direct chirping effect (see figure A6). We note that it is a global effect (i.e. a topological effect); physically, the passage from '1' to '2' is not localized, because the limit between the two regions is arbitrary. It is possible to change the line of transition in the plane (Ω, Δ) by choosing another convention which is consistent with the following off-field eigenvector. For all the chosen conventions of the chart transition line, the semi-circular path of the direct chirping necessarily crosses this transition line. The direct chirping is then an effect of the adiabatic bundle topology, since we must cover the base manifold by a minimum of two charts corresponding to the two regions. We see in this case that the direct chirping effect is not explicitly apparent in the energy-ordering convention (left of figure A4 and top of figure A6), whereas it is clear and easy to interpret in the state-ordering convention (right of figure A4 and bottom of figure A6).

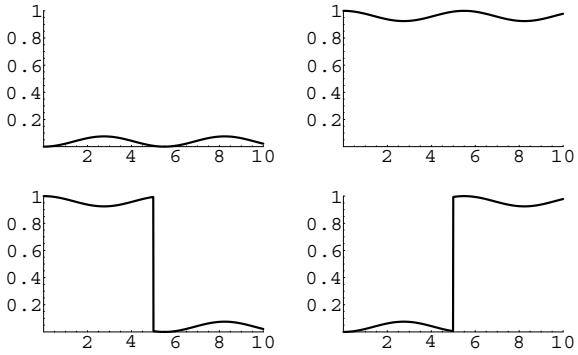

Figure A6. Up: instantaneous occupation probabilities $|\langle +, \vec{R}(t)|\psi(t)\rangle|^2$ (left) and $|\langle -, \vec{R}(t)|\psi(t)\rangle|^2$ (right). Down: instantaneous occupation probabilities $|\langle 1, \vec{R}(t)|\psi(t)\rangle|^2$ (left) and $|\langle 2, \vec{R}(t)|\psi(t)\rangle|^2$ (right), for the direct chirping dynamics. We observe small parasitic non-adiabatic transfers inducing small Rabi oscillations.

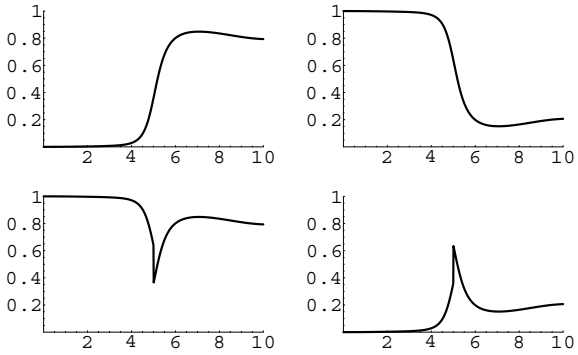

Figure A7. Up: instantaneous occupation probabilities $|\langle +, \vec{R}(t)|\psi(t)\rangle|^2$ (left) and $|\langle -, \vec{R}(t)|\psi(t)\rangle|^2$ (right). Down: instantaneous occupation probabilities $|\langle 1, \vec{R}(t)|\psi(t)\rangle|^2$ (left) and $|\langle 2, \vec{R}(t)|\psi(t)\rangle|^2$ (right), for a dynamical trajectory approaching the bound state crossing.

The non-adiabatic transitions can be located in figure A4 by considering the distribution of the monopole magnetic field. A path which passes through the black region of figure A4, even if it is traversed sufficiently slowly to be strongly adiabatic in the other regions, can induce non-adiabatic transitions. Consider, for example, the path $t \mapsto \vec{R}(t) = (\Omega(t) = 0.2\sin(\pi t/10), \Delta(t) = 1.1\cos(\pi t/10))$. With this path, we observe non-adiabatic transitions in addition to the direct chirping effect (see figure A7).

References

[1] Yatsenko L P, Guérin S and Jauslin H R 2002 *Phys. Rev.* A **65** 043407
[2] Guérin S and Jauslin H R 2003 *Adv. Chem. Phys.* **125** 147
[3] Nakahara M 1990 *Geometry, Topology and Physics* (Bristol: Institute of Physics Publishing)
[4] Wilczek F and Zee A 1984 *Phys. Rev. Lett.* **52** 2111
[5] Moody J, Shapere A and Wilczeck F 1986 *Phys. Rev. Lett.* **56** 893
[6] Li H Z 1987 *Phys. Rev.* D **35** 2615
[7] Fang Z *et al* 2003 *Science* **302** 96
[8] MacDonald A and Niu Q 2004 *Phys. World* **17** 18
[9] Bohm A *et al* 2004 *The Geometric Phase in Quantum Systems* (Berlin: Springer)

[10] Zhang P, Li Y and Sun C P 2005 *Eur. Phys. J.* D **36** 229
[11] Viennot D 2006 *J. Math. Phys.* **47** 092105
[12] Berry M V 1984 *Proc. R. Soc.* A **392** 45
[13] Hass Y, Klessinger M and Zilberg S 2000 *Chem. Phys.* **259** 121
[14] Baer M and Billing G D 2002 *Adv. Chem. Phys.* **124**
[15] Verlesi T, Vibok A, Halasz G J and Baer M 2004 *J. Phys. B: At. Mol. Opt. Phys.* **37** 4603
[16] Last I and Baer M 1985 *J. Chem. Phys.* **82** 4954
[17] Chelkowski S, Zuo T, Atabek O and Bandrauk A 1995 *Phys. Rev.* A **52** 2977
[18] Nguyen Dang T T, Châteauneuf F, Manoli S, Atabek O and Keller A 1997 *Phys. Rev.* A **56** 2142
[19] Walsh T D G, Ikov F A, Châteauneuf F, Nguyen Dang T T, Chelkowski S, Bandrauk A D and Atabek O 1998 *Phys. Rev.* A **58** 3922
[20] Aguilar J and Combes J M 1971 *Commun. Math. Phys.* **22** 269
[21] Balslev E and Combes J M 1971 *Commun. Math. Phys.* **22** 280
[22] Simon B 1972 *Commun. Math. Phys.* **27** 1
[23] Hislop P D and Sigal I M 1996 *Introduction To Spectral Theory* (New York: Springer)
[24] Reed M and Simon B 1978 *Methods of Modern Mathematical Physics IV: Analysis of Operators* (London: Academic)
[25] Moiseyev N 1998 *Phys. Rep.* **302** 211
[26] Jolicard G and Austin E J 1986 *Chem. Phys.* **103** 295
[27] Jolicard G and Perrin M Y 1987 *Chem. Phys.* **116** 1
[28] Jolicard G and Humbert J 1987 *Chem. Phys.* **118** 397
[29] Jolicard G, Leforestier C and Austin E J 1988 *J. Chem. Phys.* **88** 1026
[30] Jolicard G and Humbert J 1988 *Chem. Phys.* **127** 31
[31] Last I and Baer M 1992 *J. Chem. Phys.* **96** 2017
[32] Moiseyev N 1998 *J. Phys. B: At. Mol. Opt. Phys.* **31** 1431
[33] Riss U V and Meyer H D 1998 *J. Phys. B: At. Mol. Opt. Phys.* **31** 2279
[34] Drese K and Holthaus M 1999 *Eur. Phys. J.* D **5** 119
[35] Guérin S, Monti F, Dupont J M and Jauslin H R 1997 *J. Phys. A: Math. Gen.* **30** 7193
[36] Jolicard G, Killingbeck J P, Viennot D, Buldyreva J and Joubert P 2008 *J. Phys. A: Math. Theor.* **41** 095303
[37] Messiah A 1959 *Quantum Mechanics* vol 2 (Paris: Dunod)
[38] Nenciu G 1980 *J. Phys. A: Math. Gen.* **13** L15
[39] Simon B 1983 *Phys. Rev. Lett.* **51** 2167
[40] Dirac P A M 1931 *Proc. R. Soc.* A **133** 60
[41] Ryder L H 1980 *J. Phys. A: Math. Gen.* **13** 437
[42] Jackiw R 2002 *Preprint* hep-th/0212058
[43] Frankel T 1997 *The Geometry of Physics* (Cambridge: Cambridge University Press)
[44] Seyranian A P, Kirilliv O N and Mailybev A A 2005 *J. Phys. A: Math. Gen.* **38** 1723
[45] Last I 1984 *J. Chem. Phys.* **80** 1001
[46] Hernández E, Jáuregui A and Mondragón A 2006 *J. Phys. A: Math. Gen.* **39** 10087
[47] Mondragón A and Hernández E 1996 *J. Phys. A: Math. Gen.* **29** 2567
[48] Mondragón A and Hernández E 1997 *Preprint* quant-ph/9710018
[49] Riad Manaa M and Yarkony D R 1992 *J. Chem. Phys.* **97** 715
[50] Yarkony D R 1999 *J. Chem. Phys.* **111** 4906
[51] Yarkovy D R 2005 *J. Chem. Phys.* **123** 204101